Available online at www.sciencedirect.com
SCIENCE DIRECT
Journal of Catalysis 235 (2005) 318–326
JOURNAL OF CATALYSIS
www.elsevier.com/locate/jcat

Gas phase photocatalytic removal of toluene effluents on sulfated titania

Elodie Barraud, Florence Bosc, David Edwards, Nicolas Keller, Valérie Keller *

Laboratoire des Matériaux, Surfaces et Procédés pour la Catalyse, UMR 7515 CNRS and ELCASS (European Laboratory for Catalysis and Surface Science), Louis Pasteur University, 25 rue Becquerel, BP 08, 67087 Strasbourg cedex 2, France

Received 18 April 2005; revised 18 August 2005; accepted 19 August 2005

Available online 27 September 2005

Abstract

Photocatalytic removal of toluene in the gas phase was carried out over UV-illuminated sulfated titania materials in a cylinder-like continuous reactor. A series of SO_4^{2-}–TiO_2 samples was obtained from the addition of H_2SO_4 on an amorphous titanium hydroxide gel synthesized according to a classical sol–gel procedure. The wide variety of materials led to varying photocatalytic behaviors depending strongly on the experimental synthesis parameters, having a determinant influence on the surface specific area, the crystallinity of the material, the crystallographic nature of TiO_2, and the sulfate surface content. Optimization of the experimental parameters, such as the molarity of the sulfation solution, varying in the range 0.25–5 M leading to surface sulfate coverage of 2.5–14 wt%, and the calcination temperature ranging from 400 to 800 °C, promoted enhanced photocatalytic performance toward toluene removal as compared with commercially available P25 TiO_2 and sulfate-free sol–gel TiO_2. The most efficient photocatalyst was obtained for a near-monolayer sulfate coverage corresponding to the presence of both TiO_2 and well-dispersed SO_4^{2-} with optimized contact between SO_4^{2-} and TiO_2 domains. Furthermore, a positive role of sulfates is attributed both to an electron transfer from titanium to sulfates, leading to a positive charge trap effect, and to better desorption of electron-rich sp^2-bound carbon aromatic poisons, thus limiting deactivation.

Keywords: Titania; Sulfates; Photocatalysis; Toluene; Electron transfer; Photogenerated charge recombination

1. Introduction

The emission of volatile organic compounds by industrial processes in the United States is regulated by the Clean Air Act of 1990, which has created a strong incentive for research in this area in both the industrial and academic communities involved in innovative sustainable environmental research. Among the advanced oxidation processes developed to meet the ever-stricter antipollution legislation required by the pressure for environmental protection, photocatalytic oxidation shows much promise for the purification of contaminated wastewater containing organic pollutants and the removal of air contaminants [1–5]. Photocatalysis is advantageous because the energy required is supplied by the direct absorption of light at room temperature, which requires the use of semiconductor materials with adequate band gaps as photocatalysts. Titanium dioxide (TiO_2) is the most attractive and efficient semiconductor used today, having high photocatalytic efficiency, stability toward photocorrosion and chemicals, insolubility in water, low toxicity, and low cost. Its band gap energy of 3.2 eV leads to photoexcitation requiring wavelengths less than ca. 385 nm, corresponding to a near-UV illumination. Absorption of UV light excites electrons from the valence to the conduction band, creating electron–hole pairs with a high oxidative potential of 3 V associated with the photogenerated holes, which initiate redox reactions with adsorbed surface species [6].

Nonetheless, TiO_2 does not have sufficiently high photocatalytic activity to allow its use as such for industrial purposes. Its behavior is limited mainly by the recombination of photogenerated charges [7] and by adsorption–desorption problems of both reactants and reaction products [8]. Developing new, high-efficiency photocatalytic materials based on the TiO_2 semiconductor is thus of immense importance for sustainable development.

Heterogeneous photocatalysis has been used for the toluene degradation in either the liquid [9–11] or vapor [12–19] phase. The photocatalytic systems generally lead to moderate conver-

* Corresponding author. Fax: +33 3 90 24 27 61.
E-mail address: vkeller@chimie.u-strasbg.fr (V. Keller).

0021-9517/$ – see front matter
doi:10.1016/j.jcat.2005.08.017

sions of gaseous toluene with apparent deactivation on stream. Ollis et al. [17] reported that co-feeding of toluene with more reactive chlorinated olefins strongly increased the decomposition rate, taking inspiration from the precursor work of Bernan et al. [20], which added trichloroethylene to significantly increase the removal of nonaromatic organics. Among the alternative catalytic systems designed to improve the removal efficiency over that of pure TiO_2, a recent approach developed by Ollis et al. to avoid the hazardous use of chlorinated olefins involves pretreating the reference TiO_2 catalyst with hydrochloric acid to introduce chloride at the TiO_2 surface, leading to highly reactive and oxidizing chlorine radicals. Those radicals act in the same way as $OH^{\cdot}$ radicals and thus react with adsorbed aromatics [19]. However, the positive influence of this treatment reported by Ollis et al. is effective only for low aromatic concentrations (ca. 14 ppm, corresponding to 50 mg/m^3 in flowing air) and during the early stage of the photocatalytic reaction, with the depletion of chloride radicals contributing to catalyst deactivation [19].

Sparked by the growing worldwide interest in solid acid catalysis, mainly sulfated oxide materials and especially sulfated zirconia [21,22], sulfated titania materials recently have been used as superacid solid catalysts for several organic reactions [23,24]. However, in the photocatalysis field, several authors have emphasized that the role of the sulfate species in photocatalytic efficiency is not clear and remains controversial [25]. Indeed, Fu et al. [26] attributed the improved performance of sulfated titania for CH_3Br degradation to a greater surface area and a larger fraction of the UV photoactive anatase phase. In parallel to that finding, Muggli et al. [27] recently reported that the use of sulfated TiO_2 was nonbeneficial for the gas phase oxidation of toluene at room temperature. These authors suggested that the strong acid sites of sulfated titania play an important role by increasing the adsorption strengths and therefore the surface coverage by the organic pollutants, but also that the sulfates are detrimental to photocatalytic efficiency at room temperature and have only a positive role at temperatures above 100 °C. In addition, they showed that the photocatalytic behavior of sulfated titania was strongly dependent on the nature of the molecules to transform. Recently, Colon et al. [25] ruled out the role of any surface acidity due to the presence of sulfate groups. These authors also claimed that the sulfate species have no active role during the photocatalytic process, and that sulfation can only be considered a positive photocatalyst pretreatment that affects the TiO_2 structure by delaying its crystallization and consequently leads to stabilization of the anatase phase at higher temperatures with a rather high surface area. They reported that the photocatalytic efficiency improved with sulfation pretreatment with an increasing temperature of calcination up to 700 °C, at which point the sulfate species were removed from the material. They claimed that calcining at higher temperature eliminated much of the recombination process occurring in the crystal defects of the TiO_2 structure.

The present article reports on the use of sulfate-promoted titania for improving the efficiency of titania in room temperature photocatalytic degradation of gas phase toluene on stream. A more systematic control of the sulfation parameters is reported and demonstrates the positive role played by the sulfate species.

2. Experimental

2.1. Catalyst preparation

The sulfated titania catalysts, SO_4^{2-}–TiO_2, were prepared according to the two-step method used by Arata for sulfated oxide catalysts [21,22]. An amorphous $Ti(OH)_4$ hydroxide was prepared by a sol–gel procedure in which the $Ti[OCH(CH_3)_2]_4$ titanium isopropoxide precursor (TIP, Fluka, purum) was combined with water and ethanol at a basic pH (maintained at around 9 by dropwise addition of ammonia). After drying overnight at room temperature and further at 110 °C, the amorphous $Ti(OH)_4$ hydroxide was sulfated under vigorous stirring by an aqueous solution of sulfuric acid (VWR-Prolabo, >96.9%), using 1.5 mL of sulfation solution for 1 g of hydroxide solid. The molarity of the aqueous sulfation solution was set at 0.25, 0.5, 1, and 5 M. After evaporation of excess solution at 100 °C, the materials were further calcined in air at temperatures ranging from 400 to 800 °C for 5 h.

The performance of the sulfated titania photocatalysts as a function of the synthesis parameters is compared to that of those obtained on pure TiO_2 synthesized by the corresponding sulfate-free sol–gel procedure with calcination at 500 °C for 5 h and the TiO_2 P25 reference from Degussa.

2.2. Characterization techniques

Structural characterization was done by powder X-ray diffraction (XRD) measurements, carried out with a Siemens diffractometer (model D-5000), using a Cu-K_α radiation source in a $\theta/2\theta$ mode, with a long duration scan (10 s) and a small step scan (0.02° 2θ). The mean TiO_2 particle size (i.e., the average size of the coherent diffracting domains) was determined using Scherrer's equation with the normal assumption of spherical crystallites

$$D_c = K\lambda/b_{hkl}\cos\theta,$$

where D_c is the average particle size (nm), K is the constant of diffraction taken to be unity, λ is the X-ray wavelength (nm), and b_{hkl} is the peak width at half-maximum for the hkl peak, corrected from instrument broadening and broadening due to the K_{α_2} radiation. The content of the rutile and anatase phases was determined from the peak intensities of the most intense diffraction peaks of both the rutile and anatase phases, that is, the (110) peak at 27.6° and the (101) peak at 25.4° respectively, according to JCPDS files 21-1276 and 21-1275.

The surface area measurements were performed on a Coulter SA-3100 porosimeter using N_2 as an adsorbent. Before each measurement, the sample was outgassed at 300 °C for 3 h. Surface areas were calculated from the nitrogen adsorption isotherms using the BET method (S_{BET}). The micropore surface areas were calculated using the t-plot method [28]. A detailed study of the method, concerning the correctness of the different parameters used, has published elsewhere [29].

Thermogravimetric analysis (TGA) was performed using a SETARAM thermoanalyzer. Each sample was placed in a platinum crucible and heated from room temperature to 900 °C at a rate of 5 °C/min, using a 20% (v/v) O_2/N_2 mixture or 100% Ar at a flow rate of 100 mL/min.

X-Ray photoelectron spectroscopy (XPS) surface characterization was performed using a ThermoVG Scientific apparatus equipped with Al-K_α (1487) and Mg-K_α (1254 eV) sources (pass energy of 20 eV). All of the spectra were decomposed assuming several contributions, each having a Doniach–Sunjic shape [30] and a Shirley background subtraction [31]. Ar^+ bombardment was performed for 3 min using a source working at 2 kV and 18 mA of ionic current. The sulfur-to-titanium (S/Ti) surface atomic ratios were calculated for the sulfated titania photocatalysts using the sensitivity factors, as determined by Scofield [32]. The subtraction of the energy shift due to electrostatic charging was determined using the contamination carbon C 1*s* band at 284.6 eV as a reference.

2.3. Experimental device and procedure

The photocatalytic reaction was carried out in a 300-mm long cylindrical concentric tubular Pyrex reactor composed of two coaxial tubes 4 mm apart, between which the reactant mixture passes through. Detailed descriptions of the photocatalytic reactor and device can be found elsewhere [33,34]. Photocatalytic material (440 mg) was evenly coated on the internal side of the 35-mm diameter external tube by evaporating a catalyst-containing aqueous slurry to dryness. The catalyst-coated reactor was then dried at 110 °C for 1 h in air. Toluene (Carlo Erba, >99.5%) and water were fed at ambient temperature and atmospheric pressure by bubbling air through two saturators, then mixed with additional air (using Tylan MFC 260 mass-flow controllers) to obtain the required toluene-water-air ratios with a constant total air flow of 200 cm^3/min. The toluene content was set at 110 ppm, corresponding to 400 mg of toluene per m^3 of flowing air. The relative humidity was set at 30%, with 100% of relative humidity defined as the saturated vapor pressure of water at 25 °C, corresponding to about 24 Torr, that is, about 3% relative to the total atmospheric pressure. Before the photocatalytic reaction, the catalyst was first exposed to the polluted air stream with no illumination until dark-adsorption equilibrium was reached. Afterward, the UV illumination was switched on. Illumination was provided by a commercially available 8-W black light tube with a spectral peak centered around 380 nm, located inside the inner tube of the reactor. The reaction products were analyzed on-line every 2 min by a thermal conductivity detector on a micro-gas chromatograph (HP microCG M200H), allowing detection and quantification of toluene, water, CO_2, and organic byproducts on OV1 and Poraplot Q columns. The photocatalytic experiments were performed for 150-min durations.

3. Results and discussion

3.1. Sulfated titania characterizations

3.1.1. Structural characterizations and B.E.T determinations

Table 1 summarizes the influence of the calcination temperature of the sulfated amorphous $Ti(OH)_4$ hydroxide gel on the specific surface area, the anatase-to-rutile molar ratio, and the mean particle size, using an aqueous sulfation solution of 0.5 M molarity. The sulfated titania obtained was 0.5 M SO_4^{2-}–TiO_2. Characteristics of commercially available TiO_2 (P25; Degussa) are also given for comparison. A maximum BET specific surface area was obtained for a calcination temperature of 500 °C (i.e., 116 m^2/g), associated with an anatase mean particle size of 14 nm. Higher calcination temperatures led to a drastic decrease in surface area, down to 8 m^2/g, with a strong increase in particle size, corresponding to material sintering. A low calcination temperature (e.g., 400 °C) resulted in a lower surface area of 49 m^2/g with a mean particle size of 15 nm, which could be attributed to the low crystallinity of the sulfated material, which was proved to have a different pore network structure, due to a delay in crystallization compared with non-sulfated materials [22]. Indeed, sulfation of TiO_2 shifted the anatase → rutile phase transition toward higher temperatures, as rutile phase appeared after calcination at 600 °C on similar sulfate-free sol–gel TiO_2 [35], compared with 800 °C in our case for SO_4^{2-}–TiO_2, in agreement with the results of Colon et al. [25].

Keeping the calcination temperature at 500 °C, decreasing the molarity of the H_2SO_4 sulfation solution to 0.25 M resulted in a 71 m^2/g surface area of sulfated titania, whereas increasing the molarity to 1 and 5 M produced sulfated titania surface areas of 60 and 45 m^2/g, respectively. No significant changes in the structural characterizations was reported; only the anatase phase was observed with an unchanged anatase mean particle size (i.e., between 12 and 15 nm).

Table 1
Influence of the calcination temperature of the amorphous $Ti(OH)_4$ hydroxide gel after the sulfation procedure starting with a sulfation solution of 0.5 M, on the BET specific surface area, the anatase-to-rutile molar ratio and the mean particle size. Comparison with commercial P25 Degussa and the sol–gel TiO_2 obtained by the corresponding sulfate-free sol–gel procedure

	Calcination temperature (°C)					Commercial P25 Degussa	Sol–gel TiO_2
	400	500	600	700	800		
BET specific surface area (m^2/g) [microporous content in m^2/g derived from the *t*-plot method]	49 [0]	116 [0]	15 [0]	18 [0]	8 [0]	46 [0]	60 [0]
Anatase fraction (%)	100	100	100	100	40	80	100
Mean particle size (nm)	15	14	24	38	46	32	13

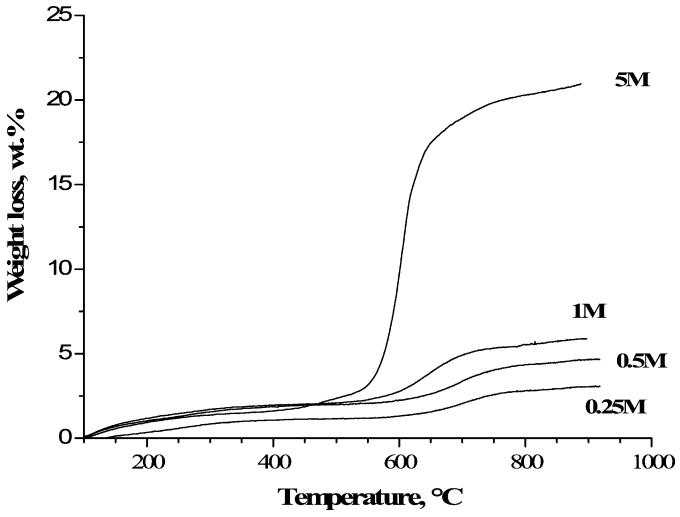

Fig. 1. Thermal gravimetry analysis of SO_4^{2-}–TiO_2 samples under air, as a function of the molarity of the H_2SO_4 sulfation solution.

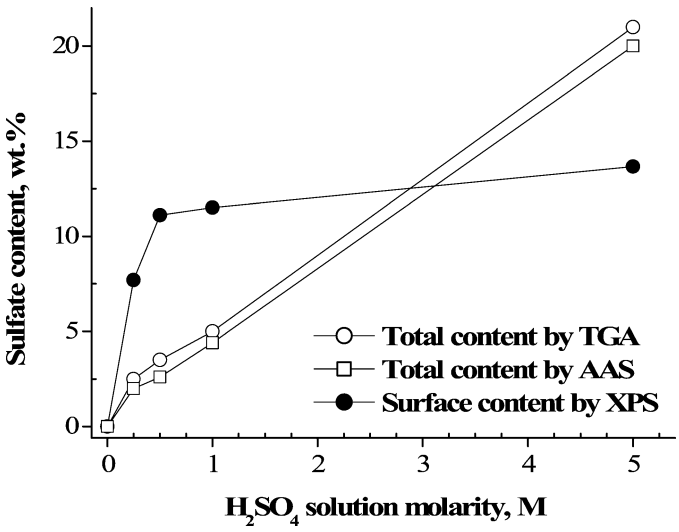

Fig. 2. Total and surface sulfate loadings as a function of molarity of H_2SO_4 sulfation solution for SO_4^{2-}–TiO_2 samples calcined in air at 500 °C for 5 h, obtained by AAS/TGA and XPS, respectively.

3.1.2. Thermogravimetric analysis

Fig. 1 shows TGA performed in air on SO_4^{2-}–TiO_2 materials synthesized using aqueous sulfation solutions of different molarities (0.25, 0.5, 1, and 5 M). The sulfated materials were stable in air at least up to 550 °C, before the weight loss occurred, attributed exclusively to the sulfate removal. The beginning of the weight loss was slightly shifted toward higher temperatures for the lowest concentration of sulfation solution. The weight loss allowed the determination of the total amount of SO_4^{2-} species, which were equal to 2.5, 3.5, 5, and 21 wt% for H_2SO_4 solutions with molarity 0.25, 0.5, 1, and 5 M, respectively. Fig. 1 thus leads to the conclusion that a progressive depletion of SO_4^{2-} started from calcination temperatures varying from 550 to 600 °C, depending on the molarity of the sulfation solution. For this reason, the standard calcination temperature in the present study was fixed at 500 °C, so as to be ensure the use and investigation of a material that is not partially desulfated. Note that the depletion SO_4^{2-} species was achieved at 800 °C in all cases. The sulfate contents determined by TGA were in close agreement with those deduced from the atomic absorption spectroscopy (AAS) measurements performed in the Service Central d'Analyse of the CNRS in Vernaison (France), both of which are shown in Fig. 2.

3.1.3. X-Ray photoelectron spectroscopy studies

Fig. 2 shows the total and surface sulfate content as a function of the molarity of the sulfation solution for samples calcined at 500 °C for 5 h. Sulfur and titanium atoms being present at the surface as SO_4^{2-} and TiO_2 species, respectively, the surface sulfate contents were deduced from sulfur-to-titanium (S/Ti) atomic surface ratios, using the appropriate molar weight-correction factors. It could be observed that the surface sulfate loading exceeded the total sulfate loading in all cases except for the 5 M sulfated material, indicating a model in which most of the sulfur should be located at the surface for low sulfation solution concentration. The incorporation of sulfates into the bulk titania framework should be more important for the highest-molarity sulfation solutions. The surface sulfate content first increased rapidly for low H_2SO_4 concentrations and more slightly for concentrations >0.5 M, whereas the total sulfate loading increased quasilinearly up to 21 wt% for the 5 M H_2SO_4 solution. The significant slowing of the slope of the curve representing the evolution of surface sulfate species could be correlated with the deposition of a monolayer of sulfate species on the titania surface. Indeed, taking into account the saturation coverage of sulfate species of 2.4×10^{18} atom/m^2, the sulfate equivalent monolayer coverage corresponds to 4.4 wt% SO_4^{2-}. The change in gradient of the surface sulfate content curve corresponds to a total sulfate content of 3.5 wt%, that is, a near-monolayer sulfate coverage. Such a double-gradient XPS pattern has already been reported for different systems like zirconia-supported tungsten oxide catalysts [36,37].

The Ti 2p XPS spectra reported in Fig. 3a show that the unsulfated TiO_2 synthesized by the analogue sulfate-free sol–gel TiO_2 procedure, taken as a reference, exhibited a signal that can be fitted with only two components, the largest one at 458.4 eV for the Ti $2p_{3/2}$ and another one at 464.1 eV for the Ti $2p_{1/2}$, corresponding to the Ti 2p spin-orbit components of Ti(IV) surface species. Comparison of the unsulfated sol–gel TiO_2 sample and the sulfated samples calcined at 500 °C for 5 h, varying in the sulfate loadings, showed an increasing upward shift of Ti 2p (IV) binding energies of 0.2, 0.4, and 0.5 eV for sulfation solution molarities of 0.25, 0.5, and 1 M, respectively, as summarized in Fig. 4. This shift to higher binding energy could be explained by the increase in effective positive charge around Ti(IV) surface species, suggesting the direct coordination of titanium atoms to strongly electron-withdrawing sulfate centers. It thus can be proposed that sulfation of TiO_2 led to the electron transfer from TiO_2 to sulfate anions. Further increasing the surface sulfate species, by increasing the molarity of the sulfation solution up to 5 M, totally annealed this upward shift, which decreased to 0 eV. The volcano curve obtained indicated that the direct coordination, and thus the effect of the

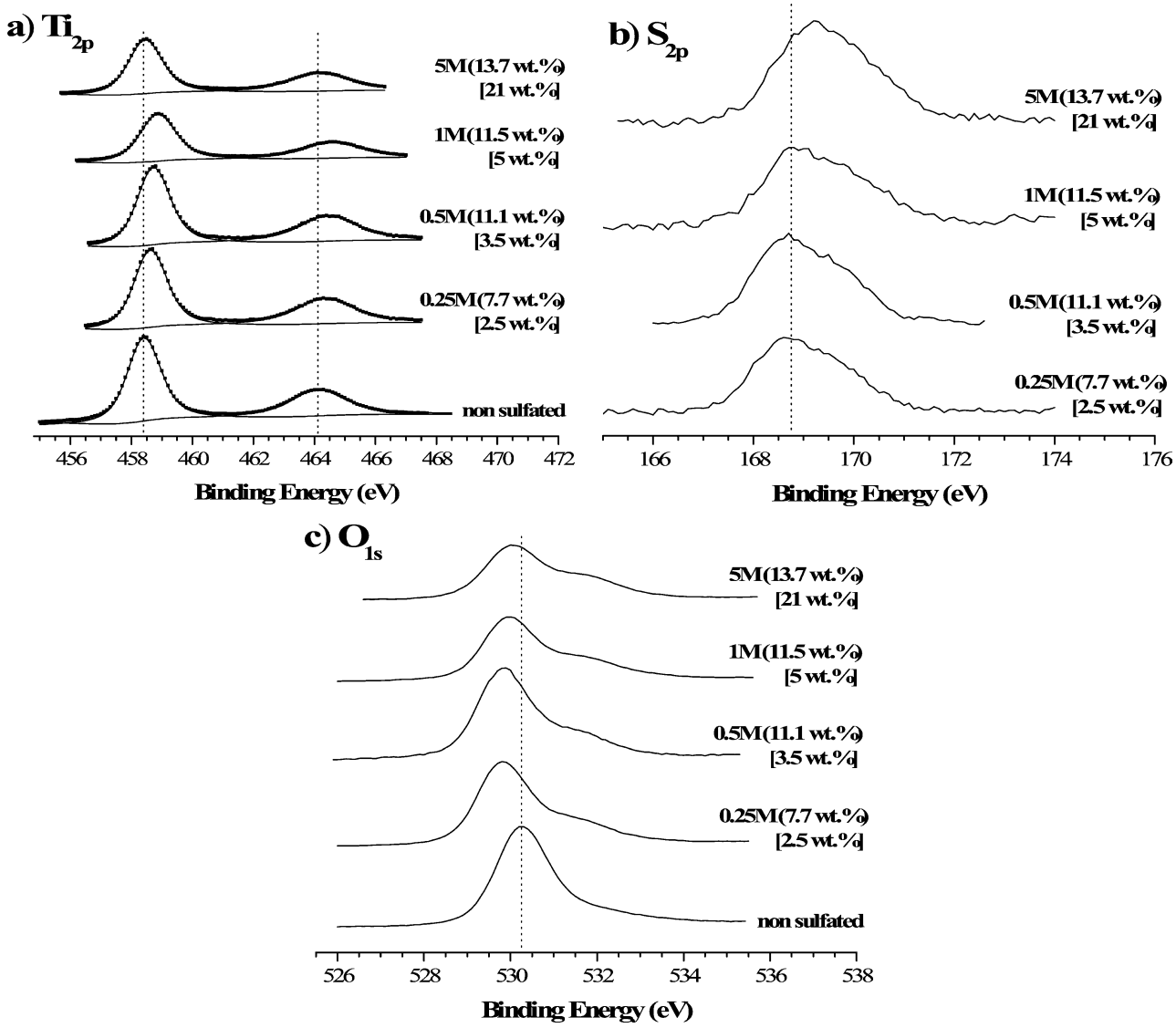

Fig. 3. XPS spectra: (a) the Ti 2*p* region of TiO_2 synthesized by the corresponding sulfate-free sol–gel procedure and sulfated-SO_4^{2-}–TiO_2 samples calcined in air at 500 °C for 5 h with different molarities of the H_2SO_4 solution; (b) the S 2*p* region of sulfated SO_4^{2-}–TiO_2 samples calcined in air at 500 °C for 5 h as a function of the molarity of the H_2SO_4 sulfation solution; (c) the O 1*s* region of unsulfated and sulfated-SO_4^{2-}–TiO_2 samples calcined in air at 500 °C for 5 h as a function of the surface sulfate loading. The surface and total amount of sulfate (wt%) are added into brackets and square brackets, respectively.

electron-withdrawing sulfate centers, was attenuated when increasing the surface sulfate levels to totally disappear on the highest-loaded sample.

The S 2*p* region of the XPS spectra (Fig. 3b; summary in Fig. 4) exhibited a broad signal with a maximum centered around 168.8 eV for the 0.25, 0.5, and 1 M SO_4^{2-}–TiO_2 catalysts, whereas the maximum for the binding energy was shifted to higher binding energies for the 5 M sulfated titania material (around 169.3 eV). This shift clearly showed a modification in the sulfur environment at the surface of the high-molarity solution 5 M sulfated titania, probably resulting from the further evolution of polysulfates to a deeper bulk sulfation. In contrast, low molarity of the sulfation solution did not influence the electronic state of sulfur atoms, meaning that the sulfur environment was similar in the resulting low-molarity sulfated materials. Similar results have been reported by Jung et al. [38]

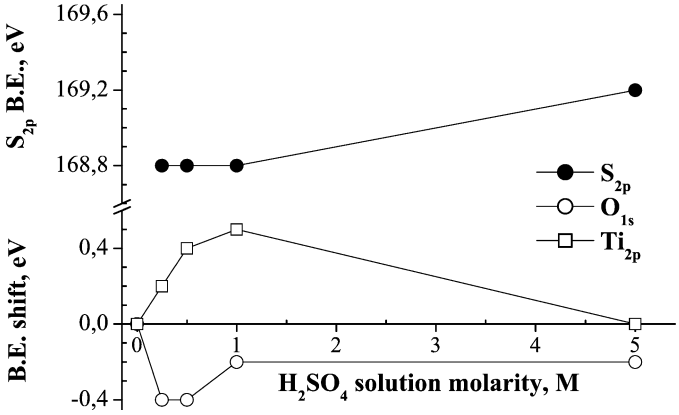

Fig. 4. S 2*p* binding energy together with the positive/negative binding energy shifts for XPS Ti 2*p* and O 1*s* contributions, as a function of the sulfation solution molarity, for the different resulting sulfated-titania materials calcined at 500 °C for 5 h.

and Ecormier et al. [39] for sulfated titania and sulfated zirconia materials, respectively, for which the binding energy of sulfur was not affected by low sulfate content, up to 6.6 and 12 wt%, respectively.

Fig. 3c shows the O 1*s* spectra obtained on the different TiO_2-based materials. The nonsulfated TiO_2 displayed a dominant peak at about 530.2 eV, corresponding to oxygen bonded to titanium atoms [40]. Sulfation of TiO_2 led to the appearance of a peak shoulder around 532 eV, assigned to oxygen bonded to the central atom of sulfur [41].

In addition, a low-molarity solution ranging from 0.25 to 1 M resulted in a slight shift toward lower energies of the titanium-bonded oxygen contribution, from 530.2 eV down to 529.8 eV (Fig. 4). This lower energy shift was weaker for higher-molarity sulfation solutions. The increase in sulfation resulted in the gradual attenuation of this main O 1*s* peak and a concomitant increase in the higher binding energy shoulder assigned to surface sulfates. For low-molarity sulfation solutions, the evolution with increasing molarity of the higher energy shift of the Ti 2*p* XPS signal, with the sulfate S 2*p* contribution kept constant, led to the hypothesis that the electron accumulation phenomena resulting from the electron transfer from TiO_2 to sulfate occurred exclusively on the oxygen atoms of the sulfate groups. Furthermore, the electron deficiency of the titanium atoms resulting from the electron transfer to sulfate led to shift the electronic density of the titanium–oxygen bond toward the electronegative oxygen atoms, and also could explain the slight shift toward lower energy of the titanium-bonded oxygen contribution at 530.2 eV. Nevertheless, increasing the molarity of the sulfation solution above 1 M decreased this binding energy shift, probably due to the appearance of new polysulfate species with different oxygen electronic states and with no electron transfer from titania to sulfate, in agreement with the Ti 2*p* XPS signal of the 5 M sample.

3.2. Photocatalytic performances of sulfated titania materials

Fig. 5 shows the photocatalytic performances for toluene removal in terms of outlet toluene concentration as a function of time on stream, with an inlet toluene concentration of 110 ppm and a relative humidity ratio of 30%, diluted in 200 ml/min flowing air. The on-stream performance of SO_4^{2-}–TiO_2 photocatalysts as a function of the calcination temperature and the sulfation solution molarity was also compared with that of the widespread commercially available TiO_2 P25 (Degussa) and the corresponding sulfate-free sol–gel TiO_2. The reference P25 photocatalyst displayed only 90% of total toluene removal and rapidly deactivated on stream. The unsulfated TiO_2 sol–gel material exhibited slightly a better activity, reaching total removal of the pollutant for only a few minutes, followed by rapid deactivation. The sulfated titania catalysts demonstrated the best efficiency for the 0.5 and 1 M sulfation solution molarity and a calcination temperature of 500 °C, with total toluene removal within 42 min before deactivation. The 0.5 M SO_4^{2-}–TiO_2 (11.1 surface and 3.5 total sulfate wt%) photocatalytic material exhibited a less pronounced deactivation than the 1 M SO_4^{2-}–TiO_2 (11.5 surface and 5 total sulfate wt%) material with time

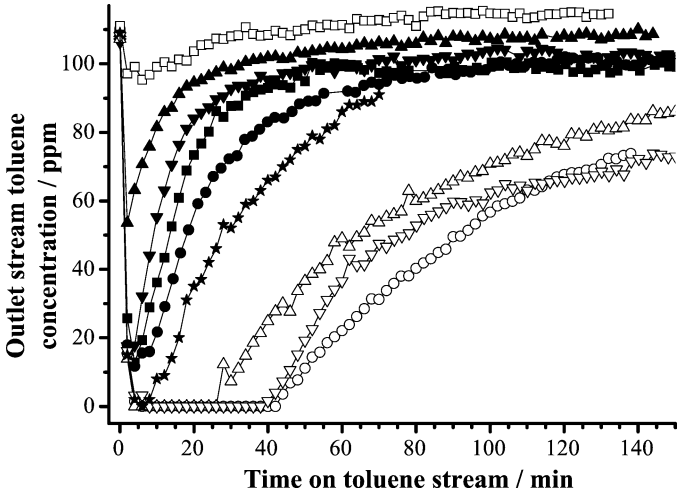

Fig. 5. Photocatalytic removal efficiency in terms of outlet toluene concentration as a function of time on stream over the commercial Degussa P25 reference catalyst (■), sol–gel TiO_2 (★), and 0.5 M-sulfated titania catalysts calcinated at 400 °C (●), 500 °C (○), 600 °C (▼), 800 °C (▲), and SO_4^{2-}–TiO_2 calcinated at 500 °C using 0.25 M (△), 1 M (▽) and 5 M (□) solutions.

on stream under UV illumination. The increased molarity of the sulfation solution up to 5 M (13.7 surface and 21 total sulfate wt%) led to a drastic decrease in the photocatalytic efficiency down to a near-zero level. In contrast, decreasing this value to 0.25 M (corresponding to a catalyst with surface and total sulfate contents of 7.7 and 2.5 wt%, respectively) yielded complete removal of toluene in 26 min. The use of calcination temperatures other than 500 °C led to photocatalysts displaying poor efficiency for the toluene removal, with decreasing performances for temperatures increasing from 400 to 800 °C.

It should be noted that, for example, the titania-based materials synthesized using 0.5 and 1 M sulfation solutions displayed total toluene removal for about 42 min, whereas they had surface areas of 116 and 60 m^2/g, respectively. In contrast, photocatalysts with similar specific surface areas demonstrated totally different photocatalytic behaviors (e.g., the 1 M SO_4^{2-}–TiO_2 and the sol–gel TiO_2 photocatalysts). Taking into account these results, the specific surface area of the materials should be ruled out from advanced hypotheses and cannot be considered a major parameter for explaining the photocatalytic efficiency for the toluene removal, with another explanation given later in this paper.

It is worth noting that only CO_2 and H_2O were detected as gaseous reaction products whatever photocatalyst was used. Fig. 6 shows the evolution of the selectivity toward CO_2 together with the toluene concentration in the outlet stream over the most efficient material, the 0.5 M SO_4^{2-}–TiO_2 sample calcined at 500 °C. An appreciable deficit in carbon occurred, suggesting the deposition of carbonaceous species on the catalyst surface. Indeed, no carbon deposition on the surface should correspond to 100% selectivity. No carbon deposit occurred, whereas the overshoot in selectivity (>100%) at the beginning of the test meant that CO_2 was formed in excess during the first period of the catalytic test. The same experiment performed without preadsorption of the toluene before illumination (i.e., by directly switching on the UV lamp when the reaction mix-

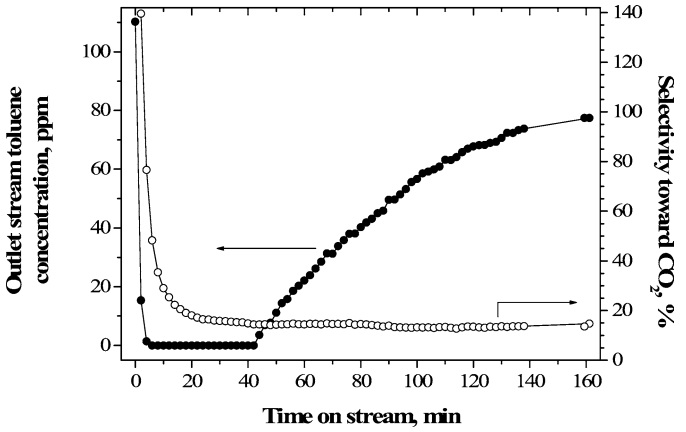

Fig. 6. Outlet stream toluene concentration in ppm and selectivity toward CO_2 on the 0.5 M SO_4^{2-}–TiO_2 catalyst calcined at 500 °C.

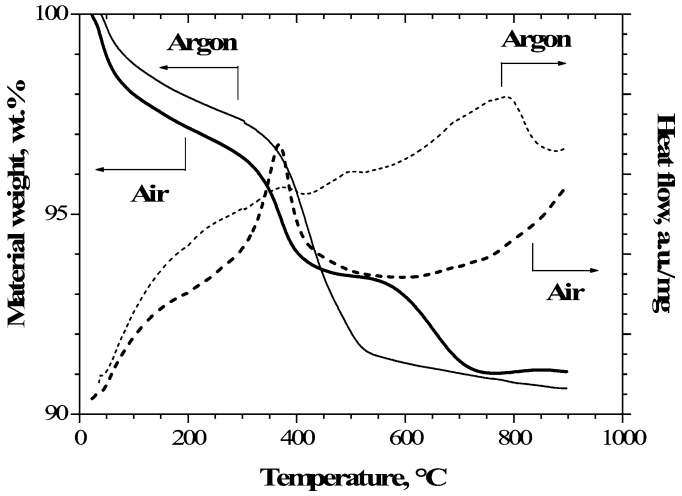

Fig. 8. TGA (Thermal Gravimetry Analysis) of the 0.5 M SO_4^{2-}–TiO_2 sample calcined at 500 °C, under air (bold) and argon (fine), after reaction of toluene.

ture passes through the reactor) yielded the disappearance of this initial CO_2 excess. This observation led to the conclusion that the initial CO_2 excess was due to the oxidation of part of the preadsorbed toluene on the fresh catalyst sample. After reaction, FTIR spectra of the 0.5 M SO_4^{2-}–TiO_2 photocatalyst calcined at 500 °C, exhibited the presence of adsorbed reaction intermediates such as benzaldehyde and benzoic acid, as shown in Fig. 7 and reported by Marci et al. [40]. Such sp^2-bound carbon aromatic molecules were poisons for the photocatalyst and thus were responsible for the catalyst deactivation by blocking the active sites. This observation led to the conclusion that the photocatalytic degradation of toluene would be mainly due to the oxidation of the methyl group (i.e., the exo-cyclic carbon–carbon bond breaking), as confirmed by complementary experiments carried out with benzene (not shown here). The improvement of the intermediate desorption on sulfated titania could lead to multiple adsorption–desorption steps for the reactant and the reaction intermediates, through the 300-mm photoreactor. The reactor can thus be considered to act as a recirculation or multiple-pass reactor. This could probably explain the absence of any reaction intermediates in the gas phase even though they were observed on the catalyst surface after testing.

From Fig. 8, showing the TGA analysis of the 0.5 M SO_4^{2-}–TiO_2 deactivated photocatalyst, it could be deduced that removal of these adsorbed reaction intermediates was possible in either air or argon, whereas the phenomenon was strongly dependent on the nature of the carrier gas. Indeed, raising the temperature in argon or in air from room temperature to 900 °C showed two or three different weight loss domains, respectively. In both cases, the weight loss in the 100–300 °C range was attributed to the desorption of adsorbed CO_2 and toluene, as observed by complementary thermodesorption experiments (not shown). Indeed, a fraction of the produced CO_2 has been reported to remain adsorbed on the photocatalyst during volatile organic compound oxidation [33,34]. It is worth

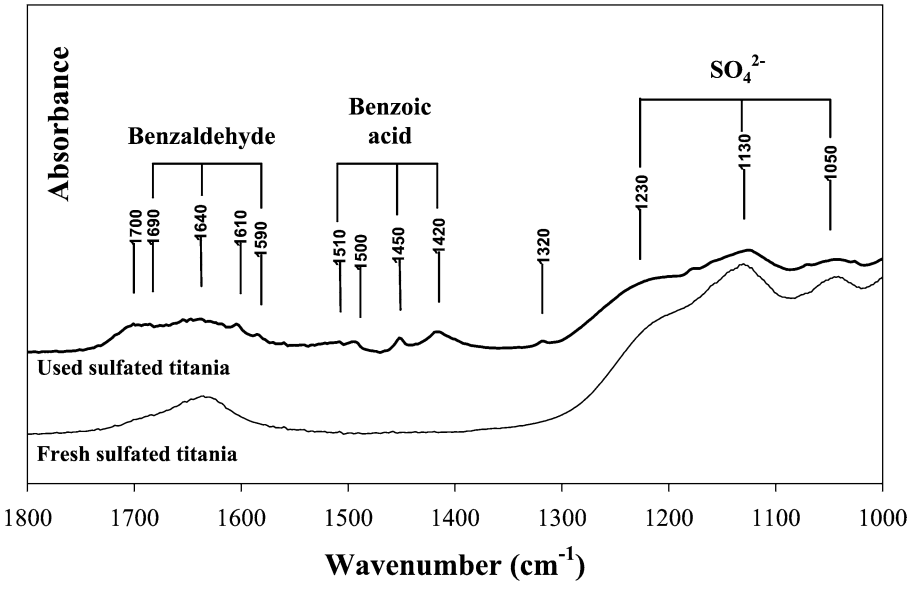

Fig. 7. Fourier Transform Infra Red spectra of the 0.5 M SO_4^{2-}–TiO_2 sample calcined at 500 °C after reaction with toluene.

noting that whatever the flowing gas, both thermal treatments yielded the same total weight loss (about 9%), meaning that the same initial species were removed from the deactivated catalyst, despite totally different behavior patterns for the weight loss and heat flow evolution. Under air, the weight loss at 300–500 °C could be assigned to the exothermic combustion of the strongly adsorbed oxygenated aromatic intermediates, before the nonexothermic removal of sulfate groups occurred at higher temperatures corresponding to the third weight loss domain, in agreement with the XPS and TGA results on fresh sulfated-titania materials. Using argon as carrier gas resulted in a unique weight loss domain at temperatures >300 °C, attributed to the simultaneous desorption of the adsorbed reaction intermediates and removal of sulfates. The removal of sulfates at a lower temperature in argon than in air could be explained by the weakening or destabilization of the oxygen-to-sulfur bond due to the desorption of the electron-rich oxygenated aromatics. Consequently, the stability in air of the sulfates at the TiO_2 surface up to 580 °C allowed regeneration of the photocatalyst to be performed by combusting the strongly adsorbed intermediates into CO_2 for 2 h at 450 °C without destroying the sulfate-containing surface. One must underline that the regeneration of the 0.5 M SO_4^{2-}–TiO_2 catalyst under air led to the restitution of the initial photocatalytic efficiency toward toluene removal.

The heat release around 700–800 °C at a constant sample weight could be assigned to the anatase-to-rutile transformation. Because the sulfate species, which are known to delay the anatase-to-rutile transformation [25,26], are released under air at a higher temperature than under argon, the heat release was observed at a higher temperature under air.

3.3. The role of the sulfate species

Sulfated titania materials led to completely different photocatalytic behaviors for the highly concentrated toluene effluent removal depending on various synthesis parameters, such as the molarity of the H_2SO_4 sulfation solution and the calcination temperature of the amorphous sulfated $Ti(OH)_4$ hydroxide. This could explain the strong discrepancy reported in the literature concerning the role of sulfates in photocatalysis and thus required a systematic control of the synthesis procedure.

Performing Ar^+ bombardment on the 0.5 M SO_4^{2-}–TiO_2 titania (not shown) led to the removal of the sulfated top layers and resulted in a drastic decrease in the S/Ti atomic surface ratio down to zero, proving the exclusive surface location of SO_4^{2-} species. This assumption is confirmed in Fig. 2, which shows the characteristic pattern of sulfated titania with strong surface anchorage at low concentration and for which a deeper bulk sulfation required a high molarity sulfation solution, as reported by Ecormier et al. [39] for SO_4^{2-}–ZrO_2 materials. Low molarity led exclusively to surface sulfation, whereas increasing the molarity solution yielded progressive formation of polysulfates and finally to bulk sulfation, as supposed for the 1 and 5 M sulfated samples, respectively, in agreement with Jung et al. [38]. In this latter case, no drastic decrease in the S/Ti atomic surface ratio was observed after Ar^+ bombardment.

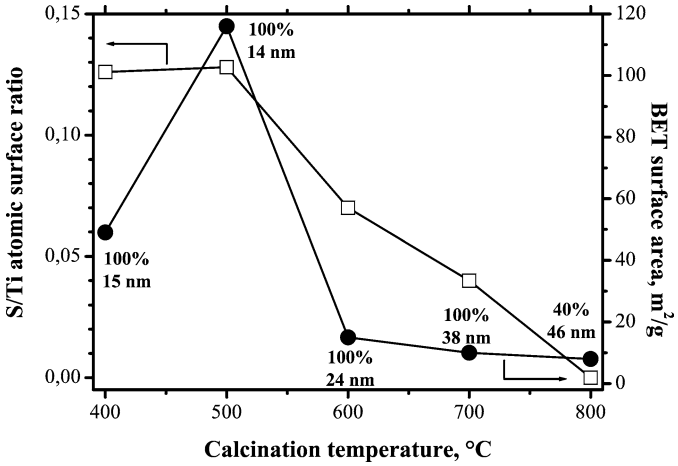

Fig. 9. Influence of the calcination temperature of the 0.5 M SO_4^{2-}–TiO_2 catalyst on the S/Ti atomic surface ratio (□), the BET surface area (●), the mean particle size derived from the XRD peak broadening using the Scherrer calculation and the anatase molar fraction.

Based on XPS analyses, the low-molarity sulfation procedure led to an electron transfer from TiO_2 to the oxygen atoms of sulfate ions, causing delocalization and a new electron distribution on the surface of TiO_2, as described by Jung et al. [38]. Those authors attributed this electron transfer to sulfate ions, leading to an electronic deficiency on Ti atoms and to the formation of Lewis acid sites. We assumed that this irreversible charge transfer acted as a charge trap [42], increasing the spatial charge separation between the photogenerated electrons and holes and thus limiting their recombination, which is one of the major limiting factors in photocatalysis. The sulfated titania catalysts with the highest shift in Ti2p binding energies showed the best photocatalytic efficiencies. Taking into account the saturation coverage of sulfate species, the optimum efficiency for toluene photocatalytic removal corresponds to a near-monolayer surface coverage of the TiO_2 surface by SO_4^{2-} species (i.e., the 0.5 M and the 1 M SO_4^{2-}–TiO_2 samples with 0.8 and 1.2 equivalent of monolayer, respectively), keeping in mind that the latter is certainly starting to built up polysulfate species.

It has been shown that an important limitation is catalyst deactivation due to strongly adsorbed sp^2-bound carbon aromatic poisons derived from benzenes, such as benzaldehyde and benzoic acid. The electron-rich nature of the sulfate species could thus favor the desorption of electron-rich sp^2-bound poisons and limit the deactivation of the photocatalyst on stream.

To summarize, a large variety of sulfated titania materials can be obtained with totally different photocatalytic behaviors depending strongly on the experimental synthesis parameters, with a main influence on the surface specific area, the crystallinity of the material, the crystallographic nature of TiO_2 (anatase or rutile), and the sulfate surface content.

Fig. 9 summarizes the influence of the calcination temperature on some physicochemical properties, including the S/Ti atomic surface ratio, BET specific surface area, anatase content, and mean particle size. For a 0.5 M sulfation solution, a maximum S/Ti atomic surface ratio was observed for materials calcined at 400–500 °C, with the material calcined at

400 °C demonstrating a lower specific surface area than the material calcined at 500 °C. Higher calcination temperatures led to a decrease in the S/Ti surface ratio, down to zero at 800 °C, due to progressive desulfation of the catalyst beginning around 600 °C, as confirmed by the TGA characterization (Fig. 1). The optimum calcination temperature can result from the highest specific surface area and good crystallinity, obtained with an adequate S/Ti atomic surface ratio (i.e., without desulfation), thus leading to higher adsorption capacity and photoefficiency.

On the optimized catalysts, the main roles of TiO_2 are in band gap excitation in the particle bulk and in reactant adsorption and transformation at the particle surface, whereas the surface sulfate groups are supposed to play a double role of a charge trap and poison desorption promoter. The explanation for this that has been put forward is that an optimum surface sulfate coverage is necessary to provide the most efficient photocatalytic material and has been found close to the equivalent monolayer coverage. This model implies that the presence of both TiO_2 and well-dispersed SO_4^{2-} with optimized contact between SO_4^{2-} and TiO_2 domains is required. Excessively high SO_4^{2-} surface coverage decreases the number of TiO_2 surface sites available for the photocatalytic reaction, whereas a low sulfate content reduces the connection (i.e., the intimate contact) between sulfate ions and TiO_2.

4. Conclusion

It has been shown that systematic control of the sulfation procedure parameters allowed optimization of the synthesis of SO_4^{2-}–TiO_2 catalysts and led to enhanced photocatalytic properties toward concentrated toluene effluent removal by both increasing the photocatalytic total efficiency and attenuating the deactivation with time on stream. The most efficient SO_4^{2-}–TiO_2 photocatalyst was obtained for a near-monolayer sulfate coverage. The positive role of sulfates has been attributed to (i) an electron transfer from titanium to sulfates, leading to a positive charge trap effect and thus hindering photogenerated electron-hole recombination, and (ii) a better desorption of electron-rich sp^2-bound carbon aromatic poisons on electron-rich sulfates, thus limiting deactivation. The better stability in air toward temperature of the sulfates compared with the aromatic deposit allowed regeneration of the photocatalyst. This halide-free sulfate-promoted TiO_2 photocatalyst is thus a regenerable and highly efficient alternative for improving the on-stream gas phase toluene removal, for which commercial TiO_2 and other alternatives lack efficiency.

Acknowledgments

This work was carried out in an “Action Concertée Incitative” framework under the auspices of the French Educational Ministry, which E. Barraud thanks for providing a postdoctoral fellowship grant. The authors are grateful to the Chemistry Department of CNRS for providing a postdoctoral fellowship grant to F. Bosc. The authors also thank M. Bacry (LMSPC) for performing the surface area measurements, D. Burger (IPCMS, UMR 7504 CNRS) and C. Petit (LMPSC) for helping with the TGA characterizations and discussions, and P. Bernhardt (LMSPC) for helping with the XPS characterizations.

References

[1] M. Schiavello (Ed.), Photocatalysis and Environment. Trends and Applications, Kluwer-Academic Publishers, Dordrecht, 1988.
[2] E. Pelizzetti, N. Serpone (Eds.), Photocatalysis. Fundamentals and Applications, Wiley, New York, 1989.
[3] D.F. Ollis, E. Pelizzetti, N. Serpone, Environ. Sci. Technol. 25 (1991) 1522.
[4] D.F. Ollis, H. Al-Ekabi (Eds.), Photocatalytic Purification and Treatment of Water and Air, Elsevier, Amsterdam, 1993.
[5] J.M. Herrmann, Catal. Today 53 (1999) 115.
[6] W.H. Strehlow, E.L. Cook, J. Phys. Chem. 2 (1) (1979) 163.
[7] B.J. Liu, T. Torimoto, H. Yoneyama, J. Photochem. Photobiol. A 113 (1998) 93.
[8] J.A. Navio, G. Colon, J.M. Herrmann, J. Photochem. Photobiol. A 108 (1997) 179.
[9] M. Fujihira, Y. Satoh, T. Osa, Nature 293 (1981) 206.
[10] A. Navio, M. Garcia Gomez, M.A. Pradera Adrian, J. Fuentes Mota, J. Mol. Catal. 104 (1996) 329.
[11] L. Cao, Z. Gao, S.L. Suib, T.N. Obee, S.O. Hay, J.D. Freihaut, J. Catal. 196 (2000) 253.
[12] T. Ibusuki, K. Takeuchi, Atm. Environ. 20 (9) (1986) 1711.
[13] T.N. Obee, R.T. Brown, Environ. Sci. Technol. 29 (1995) 1223.
[14] V. Augugliaro, S. Coluccia, V. Loddo, G. Martra, L. Palmisano, M. Schiavello, Appl. Catal. B 20 (1999) 15.
[15] V. Augugliaro, V. Loddo, G. Marci, L. Palmisano, C. Sbriziolo, M. Schiavello, M.L. Turco Liveri, Stud. Surf. Sci. Catal. 130 (2000) 1973.
[16] H. Einaga, S. Futamura, T. Ibusuki, Appl. Catal. B 38 (2002) 215.
[17] O. d’Hennezel, D.F. Ollis, J. Catal. 167 (1997) 118.
[18] O. d’Hennezel. PhD thesis, North Carolina State University, 1998.
[19] M. Lewandowski, D.F. Ollis, J. Catal. 217 (2003) 38.
[20] E. Berman, J. Dong, in: W.W. Eckenfelder, A.R. Bowers, J.A. Roth (Eds.), 3rd Int. Symp. Chem. Oxidation, Technologies for the Nineties, vol. 3, Technomic, Lancaster, PA, 1993, p. 183.
[21] K. Arata, Appl. Catal. 146 (1996) 3.
[22] K. Arata, Adv. Catal. 37 (1990) 165.
[23] L.K. Noda, R.M. De Almeida, L.F.D. Probst, N.S. Gonçalves, J. Mol. Catal. A 225 (2005) 39.
[24] A. Corma, A. Martinez, C. Martinez, Appl. Catal. A 144 (1996) 249.
[25] G. Colon, M.C. Hidalgo, J.A. Navio, Appl. Catal. B 45 (2003) 39.
[26] X. Fu, Z. Ding, W. Su, Chin. J. Catal. 20 (1999) 321.
[27] D.S. Muggli, L. Ding, Appl. Catal. B 32 (2001) 181.
[28] E.P. Barrett, L.G. Joyner, P.H. Halenda, J. Am. Chem. Soc. 73 (1951) 373.
[29] R.S.H. Mikhail, S. Brunauer, E.E. Bodor, J. Colloid Interface Sci. 26 (1968) 45.
[30] S. Doniach, M. Sunjic, J. Phys. C: Solid State Phys. 3 (2) (1970) 285.
[31] D.A. Shirley, Phys. Rev. B 5 (1972) 4709.
[32] J.H. Scofield, J. Electron. Spectrosc. Relat. Phenom. 8 (1976) 129.
[33] V. Keller, F. Garin, Catal. Commun. 4 (2003) 377.
[34] V. Keller, P. Bernhardt, F. Garin, J. Catal. 215 (2003) 129.
[35] N. Keller, V. Keller, E. Barraud, F. Garin, M.J. Ledoux, J. Mater. Chem. 14 (12) (2004) 1887.
[36] F. Di Gregorio, V. Keller, J. Catal. 225 (2004) 45.
[37] Y. Xie, Y. Tang, Adv. Catal. 37 (1990) 1.
[38] S.M. Jung, P. Grange, Catal. Lett. 76 (2001) 1.
[39] M.A. Ecormier, K. Wilson, A.F. Lee, J. Catal. 215 (2003) 57.
[40] G. Marci, M. Addamo, V. Augugliaro, S. Coluccia, E. Garcia-Lopez, V. Loddo, G. Marta, L. Palmisano, M. Schiavello, J. Photochem. Photobiol. A 160 (2003) 105.
[41] S.M. Jung, P. Grange, Catal. Today 59 (2000) 305.
[42] R. Gomez, T. Lopez, E. Ortiz-Islas, J. Navarrete, F. Tzompanztzi, X. Bokhimi, J. Mol. Catal. A 193 (2003) 217.